Chronostratigraphy and Paleoclimatology of the Lodève Basin, France: Evidence for a Pan-Tropical Aridification Event across the Carboniferous – Permian Boundary

Lauren A. Michel[1], Neil J. Tabor[2], Isabel P. Montañez[3], Mark Schmitz [4], Vladymir I. Davydov [4]

[1]Perot Museum of Nature and Science, 2201 N. Field Street, Dallas, TX 75201-1704

[2] Roy M. Huffington Department of Earth Sciences, Southern Methodist University, PO Box 750395, Dallas, TX 75275-0395, USA

[3]Department of Earth and Planetary Sciences, University of California, Davis, California 95616, USA

[4]Department of Geosciences, Boise State University, Isotope Geology Laboratory, Boise, Idaho 83725, USA

[5] Kazan Federal University, 18 Kremlyovskaya St., Kazan 420008, Republic of Tatarstan, Russian Federation

Corresponding author: lauren.michel@perotmuseum.org, t:(214) 756-5786, f: (214) 756-5890

ABSTRACT

Paleosols preserved within the Carboniferous – Permian succession of the Lodève Basin, Massif Central, France change stratigraphically from Histosols to calcic Vertisols and Calcisols to gypsic Vertisols and ultimately back to calcic Vertisols and Calcisols. New high-precision U-Pb zircon ages (CA-IDTIMS) for tuff beds within the Lodève and adjacent Graissessac basins significantly revise the chronostratigraphy of these and

correlated Permian terrestrial basins of eastern Euramerica. Under the newly revised chronostratigraphy presented here these stratigraphic changes in morphology indicate a substantial drying of paleoenvironments across the Carboniferous – Permian boundary with a trend toward progressively more arid and seasonal climates through most of the early Permian. This newly-realized chronology provides a paleoenvironmental and paleoclimatic timeline for eastern tropical Pangea that is contemporaneous with similar records in western Pangea and suggest pan-tropical, progressive climate change toward aridity and seasonality occurred from the Late Carboniferous through early Permian.

Keywords: Paleoclimate; Carboniferous; Permian; Paleosols; Lodève Basin

1. Introduction

There is a first-order correlation between atmospheric pCO_2 concentrations and global climate throughout the past half billion years (Royer et al., 2004). As present-day CO_2 increases there is a need to assess the effects of climate change in a warming world. Because the Carboniferous – Permian is the last icehouse to greenhouse transition on a vegetated and metazoan-populated Earth, and this time period corresponds to an increase in atmospheric CO_2 concentrations (Montañez et al., 2007), there has been a focus on reconstructing global terrestrial paleoclimate across this transition interval (e.g., Cecil, 1990; Cecil, 2003; DiMichele, 2014; DiMichele et al., 2006; Montañez et al., 2007; Peyser and Poulsen, 2008; Tabor et al., 2004; Tabor et al., 2013; Tabor and Poulsen, 2008). While Carboniferous – Permian terrestrial paleoclimate reconstructions based on paleosol records have emerged from the western tropics (Rosenau et al., 2013a; Rosenau et al., 2013b; Tabor and Montañez, 2004) and high latitudes (Beauchamp, 1994; Gulbranson et al., 2010; Gulbranson et al., in press; Limarino et al., 2014), only recently have proxy records of this nature been constructed for central and eastern tropical regions of Pangaea (Eros et al., 2012; Schneider et al., 2006; Thomas et al., 2011). Existing paleoclimate reconstructions from western tropical Pangea indicate the onset of seasonality toward the close of the Carboniferous and a clear aridification trend through the early Permian (Bishop et al., 2010; Tabor and Montañez, 2002; Tabor et al., 2008). While, there are hints of this aridity trend seen in eastern Ukraine during the Carboniferous – Permian boundary (Eros et al 2012), the long-term trend of this aridity through the Permian is unknown. At this time it remains unclear if this paleoclimate trend is limited to the western tropics or if it extends throughout the tropics. The Lodève

Basin in the south of France was chosen as an ideal location to extend Carboniferous – Permian climate trends from the western, to the central, Pangean landmass because of previously developed stratigraphic and paleoecological frameworks and the presence of multiple ashes throughout the succession (Körner et al., 2003; Pochat and Van Den Driessche, 2011; Schneider et al., 2006).

Presented herein are new chronostratigraphic constraints and paleosol data for the Carboniferous – Permian formations of the Lodève and adjacent Graissessac Basins, southern France. The new chronostratigraphy places the majority of the basin infill within the Ghzelian to upper Sakmarian. Changes in paleosol micro- and macromorphology indicate a change from humid everwet climates in the latest Carboniferous to seasonal and semiarid climates, with a progressive trend toward aridity, through the early Permian. Therefore, this study documents a similar and contemporaneous climate trend in central Pangea as seen in previous climate reconstructions from western tropical Pangea, supporting a pan-tropical aridification during this interval of time, which may have occurred in response to rising levels of atmospheric CO_2 (e.g., Montañez et al., 2007).

2. Background

2.1 Geological Setting

The Lodève Basin is situated to the NW of Montpellier, France, on the southeastern edge of the French Massif Central (Fig. 1). The basin covers a total area of approximately 150 km^2 (Fig. 1), and lies upon Precambrian and Cambrian rocks composed of schists, arkosic and quartzose sandstones, limestones and volcaniclastics (Conrad and Odin, 1984). Four bounding-faults delimit the Lodève Basin and define its characteristic half-graben shape. In particular, vertical motions along the southern, E-W

trending Les Aires fault were responsible for creation of accommodation and sediment accumulation during Permian time (Conrad and Odin, 1984). During the Pennsylvanian and Permian the Lodève Basin occupied a low latitude (0 to 10°N) (Fig. 1B) position on the Pangean landmass approximately 400 km inland from the Tethys ocean (Schneider et al., 2006). During this time, the Hercynian Mountains, of unknown topography (Ziegler et al., 1997) separated the Lodève Basin from Tethys. Paleomagnetic studies of the Lodève Basin strata indicate that it was a site of paleogeographic stability throughout the Permian, whereas surrounding contemporaneous basins underwent a component of rotation (Chen et al., 1997; Cogné et al., 1990; Diego-Orozco and Henry, 1993; Henry et al., 1999).

Lodève Basin fill consists of ~3000 m of Carboniferous – Permian siliciclastics previously thought to range from Ghzelian through Changhsingian (Zechstein) age, with unconformities that separate (1) the lower Asselian from upper Asselian strata and (2) the middle Sakmarian from upper Artinskian strata (upper Lower Rotliegend to the lower Upper Rotliegend I; Schneider et al., 2006). Only Permian strata outcrop in the Lodève Basin. However, Carboniferous outcrops occur in the adjacent Graissessac Basin to the west of the Lodève Basin (Bruguier et al., 2003). These western outcrops include Gzhelian (Stephanian C) through Lower Asselian (early Lower Rotliegend) strata.

Prior radioisotope age constraints for the Lodève and correlative Permian basins of southern France are sparse, and limited to relatively imprecise SIMS U-Pb zircon ages, SHRIMP U-Pb zircon ages or $^{40}Ar/^{39}Ar$ sanidine and biotite ages. SIMS $^{206}Pb/^{238}U$ ages on zircons from five volcanic ash layers located in the southern French Massif Central basins, including a tonstein from the Graissessac, record an average regional magmatic

106 activity from 295.5 ± 5.1 to 297.9 ± 2.1 Ma and constrain the age of the Graissessac
107 Basin to the Late Carboniferous (295.3 ± 4.8 Ma) early Permian (Autunian to
108 Sakmarian); (Bruguier et al., 2003). Schneider and others (2006) developed a
109 biostratigraphy for younger Permian strata in the Lodève Basin to constrain the timing of
110 deposition given the lack of chronostratigraphic constraints (Fig. 2). Schneider and
111 others (2006) also referenced unpublished U-Pb zircon ages for the Viala Formation
112 (289.3 ± 6.7 Ma) and Octon Member of the Salagou Formation (284 ± 4 Ma) in the
113 Lodève Basin, but provide no data or analytical details. Breitkreuz and Kennedy (1999)
114 and Königer et al. (2002) presented SHRIMP U-Pb zircon ages for volcanics within
115 Carboniferous - Permian transition sediments of several German basins, ranging from
116 302 to 297 (± 3) Ma. Several $^{40}Ar/^{39}Ar$ dates in the range of 302 to 291 Ma from
117 Carboniferous – Permian basins of east-central Europe have been published (Burger et
118 al., 1997; Goll and Lippold, 2001; Hess and Lippolt, 1986); however, the accuracy of
119 these dates has been questioned by direct comparison to high-precision U-Pb zircon ages
120 in recent studies (Davydov et al., 2010; Gastaldo et al., 2009).
121 Carboniferous – Permian strata of the Lodève Basin underwent extensive
122 alteration in response to deep burial and higher-than average geothermal heat flow in the
123 region. Copard and others (2000) report T_{max} burial temperatures between 600 – 610°C
124 for the western Graissessac Basin based on vitrinite reflectance data of coals and
125 suggested that Carboniferous – Permian heat flow was 180mW/m^2, a value that is 4.5
126 times the average heat flow value in typical stable cratonic basins (Blackwell, 1971;
127 Condie, 1997). Copard and others (2000) interpreted such high heat flow values, and thus
128 the high-temperature burial history, in the Graissessac Basin to a regional high-

129 temperature event associated with the end-Permian Saalic Orogeny. In addition, Buatier
130 and others (2000) identified nacrite, a high-temperature polymorph of kaolinite (Hanson
131 et al., 1981; Shen et al., 1994), as a burial diagenetic mineral that formed within
132 dolomitic strata in the basement rocks of the Lodève Basin. In the basin, the nacrite
133 appears to form contemporaneously with hydrothermal barite. Fluid inclusion data from
134 these barites indicates these minerals formed in the presence of a high-salinity brine (25
135 wt% NaCl) at temperatures ranging from 80 to 100°C (Buatier et al., 2000).

136 **2.2 Lithostratigraphy**

137 The lithostratigraphy of the Lodève Basin may be divided into three ascending
138 units. Unit I consists of coal-bearing strata of the Graissessac Formation (Fig. 2). Unit II
139 consists of fluvio-alluvial siliciclastics of the Usclas St. Privat, Tuilieres-Loiras, and
140 Viala formations; Unit III includes the Rabejac, Salagou and La Lieude formations. (Figs.
141 2,3). The Rabejac Formation is composed of fluvio-alluvial siliciclastics, whereas, the
142 overlying Salagou Formation includes mixed playa siliciclastics, evaporites and zeolites
143 (Schneider et al. 2006). The overlying La Lieude Formation is composed of siliciclastics
144 deposited within fluvio-alluvial environments (Schneider et al. 2006).

145 **2.3 Previous paleoclimate studies**

146 Previous studies of the whole rock chemical composition of the Permian strata
147 within the Lodève Basin were used as indicators of climate-sensitive minerals such as
148 analcime and albite (Schneider et al., 2006). Stratigraphic variations in whole rock
149 chemistry indicate an increase in analcime and albite in the Octon Member of the Salagou
150 Formation that was interpreted to represent a strongly evaporitic environment in a semi-
151 arid climate (Schneider et al., 2006). Schneider and others (2006) and Quast and others

(2006) further used the stable carbon and oxygen isotopic compositions of carbonate cements in sandstones and calcretes in Permian strata of the Lodève Basin as potential paleoclimate proxies. Both studies concluded that the carbonates were diagenetically overprinted and not appropriate for paleoenvironmental reconstruction.

Pochat and Van Den Driessche (2011) built upon previous studies in other continental rift basins (Harris et al., 2004; Lambiase, 1990; Lefournier, 1980; Pochat et al., 2005; Prosser, 1993; Schlische, 1991) to develop a model of lacustrine sedimentation in the Lodève Basin. Their model hypothesizes that lake water volumes did not change substantially throughout the Carboniferous – Permian, but that lake surface areas did change. Pochat and Van den Driessche (2011) attributed the changes in the composition of sedimentary fill of the Lodève Basin to changes in tectonic style associated with typical rift basin development as opposed to changes in Carboniferous – Permian paleoclimate.

3. Methods

3.1 Field Methods

Fieldwork included identification and description of paleosols using modern soil description techniques (Schoeneberger et al., 2012) as advocated for paleosols (Retallack, 1988), and placement of these paleosols into an existing stratigraphic framework (Körner et al., 2003; Schneider et al., 2006). Outcrops were trenched back to remove surficial weathering and samples were collected for petrographic analysis. Layers preserving evidence for paleopedogenesis were logged and described in detail according to previously defined methods (Tabor and Montañez, 2004; Tabor et al., 2006). Paleosol

175 profile tops were identified on the basis of a marked change in grain size and color, as
176 well as preservation of primary sedimentary structures. Profile bases were delineated at
177 the lowest occurrence of unaltered parent material. Paleosol matrix was sampled at 0.1-
178 0.2 m vertical spacings; rhizoliths and paleosol nodules were sampled where present.
179 Paleosol classification primarily follows the system of Mack and others (1993). Paleosol
180 types, as well as the names and stratigraphic positions of collected samples, are provided
181 in Figure 3. Micromorphological analysis of thin sections (n=46) followed the methods
182 developed for modern soils (Bullock et al., 1985; Stoops, 2003; Stoops et al., 2010).

183 **3.2 Radiometric Dating**

184 Volcanic strata (tuffs, tonsteins, and cinerites) were identified and sampled in the
185 field utilizing the stratigraphy summarized by Schneider and others (2006) and references
186 therein. Abundant populations of prismatic zircon crystals were separated from hand
187 samples of each volcanic horizon by conventional density and magnetic methods.
188 Methods for U-Pb geochronology using chemical abrasion isotope dilution thermal
189 ionization mass spectrometry (CA-IDTIMS) follow those previously published by
190 Davydov et al. (2010) and Schmitz and Davydov (2012). A fraction of the zircon separate
191 from each sample, which was selected on the basis of sharply facetted morphology,
192 clarity and lack of inclusions, was placed in quartz beakers in a muffle furnace at 900°C
193 for 60 hours to anneal minor radiation damage; in preparation for subsequent chemical
194 abrasion (Mattinson, 2005). Single zircon crystals were individually subjected to a
195 modified single step, high-T (12 hours at 180°C) version of the chemical abrasion
196 method of Mattinson (2005). U-Pb dates and uncertainties for each analysis were
197 calculated using the algorithms of Schmitz and Schoene (2007) and the U decay

198 constants of Jaffey and others (1971). Uncertainties are based upon non-systematic
199 analytical errors, including counting statistics, instrumental fractionation, tracer
200 subtraction, and blank subtraction. These error estimates should be considered when
201 comparing our $^{206}Pb/^{238}U$ dates with those from other laboratories that used tracer
202 solutions calibrated against the EARTHTIME gravimetric standards. When comparing
203 our dates with those derived from other decay schemes (e.g., $^{40}Ar/^{39}Ar$, ^{187}Re-^{187}Os), the
204 uncertainties in tracer calibration (0.05%; Condon et al., 2007) and U decay constants
205 (0.108%; Jaffey et al., 1971) should be added to the internal error in quadrature. Quoted
206 errors for calculated weighted means are thus of the form ±X(Y)[Z], where X is solely
207 analytical uncertainty, Y is the combined analytical and tracer uncertainty, and Z is the
208 combined analytical, tracer and ^{238}U decay constant uncertainty.
209
210 **4. Results**
211 **4.1 Field**
212 Paleosols in the Lodève Basin exhibit variations in characteristics such as texture,
213 color, structure, presence and concentration of soil-forming minerals, and accumulations
214 of organic matter. Based upon field observations of these characteristics, there are five
215 different types of paleosols in the Permian-Carboniferous strata of the Lodéve Basin:
216 Histosols, Calcisols, calcic Vertisols, gypsic Vertisols and Protosols (Figs. 4, 5, 6A-F).
217 Protosols found in the basin are not useful for paleoclimate reconstruction and are not
218 discussed further herein.
219 Histosols (n=7) are found only in the Stephanian Graissessac Formation Histosols
220 occur as seven discrete coal seams, which range in thickness from 1.2 to 5.2 m thick

221 (Figs. 4, 5A). Each seam is stratigraphically separated by intercalated claystones,
222 siltstone and volcanic ash layers. The mineral Jarosite occurs through all strata.
223 Calcisols (n=2) occur in the Tuilieres-Loiras and La Lieude formations. (Figs.
224 3,4). Calcisols of the Lodève Basin are identified based on the presence of stage II
225 through stage IV pedogenic carbonate accumulation (Machette, 1985; Mack et al., 1993).
226 Stage II carbonate accumulation includes mm- to cm-sized carbonate nodules and
227 tubules, whereas Stage III and Stage IV carbonate accumulation includes continuous
228 lateral horizons of carbonate cementation (Machette, 1985). These soils preserve original
229 sedimentary structure to massive structure and are often truncated by overlying cross-
230 bedded sandstones. Soils with groundwater carbonate nodules were identified based on
231 the presence of inclusive growth of carbonate cements around siliclastic grains and
232 laminations from suspension settling of grains (Fig. 5B); these carbonates noduless were
233 excluded from the study.
234 Calcic Vertisols (n= 4) occur in the Viala Formation, Octon Member of the
235 Salagou Formation, and in the La Lieude Formation (Figs. 3, 4, 5C, D). These paleosols
236 are identified based on the presence of prominent features resulting from shrink-swell
237 processes as well as pedogenic accumulation of subsurface calcium carbonate. Paleosols
238 in the Lodève Basin contain features indicative of shrink-swell processes including
239 slickensides (Fig. 5C), clastic dikes (Fig. 5D), and wedge- shaped aggregates, as well as
240 carbonate nodules and tubules. These paleosols are broken into multiple horizons. The
241 lower-most horizons are often massive to platy, dusky red (5YR 5/4 – 2.5YR 3/4)
242 mudstones that in some locations are calcite cemented. The upper boundary varies from
243 abrupt and wavy to clear and smooth. Overlying the lower horizons are between 1 to 3

244 horizons containing common stage II pedogenic carbonate nodules that usually increase
245 in abundance down profile. These horizons are dusky red (2.5 YR 3/4 – 10YR 4/4), silty
246 mudstones to mudstones with angular blocky structure and slickensides. The upper
247 boundary is typically abrupt and wavy and possesses clear mukkara subsurface
248 expression. Where not truncated, the overlying horizons are weak red (7.5R 4/3) silty
249 mudstones to mudstones. Some horizons are massive while others have angular blocky
250 structure and slickensides and desiccation cracks infilled by sandstone that extend up to
251 80 cm below the paleosol surface. These soils are often 1 to 2 meters thick and are
252 typically truncated by cross-bedded sandstones.
253 Vertic Gypsisols (n=2) are paleosol profiles that occur in the upper Merifons
254 Member of the Salagou Formation and lower La Lieude formations. (Figs. 3, 4, 5E, F).
255 They are composed of two horizons; the lower horizon is mostly massive red mudrock
256 (7.5 R 3/3) with the lower ~ 5 cm defined by thin platy structure and satin-spar calcite
257 cements. This satin-spar texture is not typically attributed to calcite cement, but is
258 commonly found in gypsum (Gustaveson 1990). Therefore, we interpret this texture as
259 being originally gypsum in the soil-forming environment. The upper boundary between
260 horizons is abrupt and wavy to broken due to the presence of vertically oriented clastic
261 dykes. Overlying the horizon is a 2 – 3 cm thick greenish-gray (G1 6/5G) laminated
262 coarse silt ot fine sand (Fig. 5E, 5F) The upper boundary is abrupt and smooth, and is
263 commonly overlain by another vertic Gypsisol in the upper Salagou (Merifons Member).
264 The most prominent feature is the accumulation of original pedogenic gypsum, but also
265 exhibit vertic features such as clastic dikes that extend downward from the interpreted

paleosurface (Mack et al., 1993). They also have weakly developed soil structure. The paleosol profiles are intercalated with laminated coarse silt to fine sandstones (Fig. 5F).

4.2 Micromorphology

Micromorphology of Calisols, calcic Vertisols, and vertic Gypsisols reveals evidence of biological processes including orabated mite fecal material (Fig. 6A), bacterial films, primary boxwork fabric originating from bacterial processes (Von Der Borch et al., 1977), which now have been altered to microspar and dolomite (Fig. 6B) and rooting (Fig. 6C). Calcic Vertisols also show clotted micrite textures (Fig. 6D) and wedge-shaped aggregates with Fe-oxide-stripping and concentrations (Fig. 6F). Additionally, the calcic Vertisols preserve hematite after primary clay fabric while the vertic Gypsisols have both hematite coatings after primary clay as well as illuvated clay coatings along roots (Fig. 6E). The Vertic Gypsisols have been diagenetically altered and the gypsum has been replaced by calcite spar cement (Fig. 6E).

4.3 U-Pb geochronology

4.3.1 *Graissessac Formation*

Eleven single zircon grains were analysed from a tonstein collected from coal bed 4 (Monte Sénégra 3; Fig. 7). Four anomalously older or younger zircons are interpreted as either bearing an inherited core component, or containing residual Pb-loss domains. Seven other grains yielded a cluster of equivalent U-Pb isotope ratios, with a calculated weighted mean $^{206}Pb/^{238}U$ date of 304.07 ± 0.07(0.17)[0.36] Ma (MSWD = 0.71), which is interpreted as the eruption and depositional age of the tonstein.

Nine single zircon grains were analyzed from a tonstein collected from coal bed 5 (Monte Sénégre 2; Fig. 7), which was approximately 20 m above Monte Sénégra 3. One

289 slightly older discordant analysis is interpreted as containing an inherited core, while two
290 anomalously younger grains may have residual Pb-loss. Six single grains yielded a
291 cluster of dates that are equivalent with a weighted mean $^{206}Pb/^{238}U$ date of 303.95 ±
292 0.08(0.17)[0.36] Ma (MSWD = 1.4). This date is interpreted as the eruption and
293 depositional age of the tonstein. While slightly younger than the underlying tonstein from
294 coal bed 4, the two tonstein ages are within analytical uncertainty thus establishing rapid
295 depositional rates through this interval of the Graissessac Formation
296 4.3.2 *Tuilières–Loiras Formation (Loiras Member)*
297 Eleven single zircon grains were analyzed from tuff bed V, which is in the upper
298 portion of the middle Loiras Member (Figs. 3, 7). Five older analyzed grains are
299 interpreted as reworked crystals from previous eruptions or containing inherited core
300 components. Six single grains yielded a cluster of youngest dates that are equivalent with
301 a weighted mean $^{206}Pb/^{238}U$ date of 293.94 ± 0.08(0.16)[0.35] Ma (MSWD = 0.81). This
302 date is interpreted as the eruption and depositional age of the tuff.
303 Thirteen single grains from the overlying tuff bed VI (Figs. 3, 7) yielded a cluster
304 of ten concordant and equivalent zircon grains, with a weighted mean $^{206}Pb/^{238}U$ date of
305 293.85 ± 0.10(0.17)[0.36] Ma (MSWD = 1.49). This date is interpreted as the eruption
306 and depositional age of the tuff. Three variably younger analyzed grains are interpreted as
307 containing residual Pb-loss domains.
308 4.3.3 *Viala Formation*
309 Twenty single zircon grains were analyzed from a sample taken from tuff bed III,
310 which is approximately 60 meters above the base of the Viala Formation (Fig. 3). Ten of
311 those analyses spread along the concordia curve with ages from 292.2 to 294.4 Ma and

312 are interpreted as containing variable inherited components. Three anomalously younger
313 grains may have residual Pb-loss. The remaining seven single grains yielded a cluster of
314 dates that are equivalent with a weighted mean $^{206}Pb/^{238}U$ date of 290.96 ±
315 0.19(0.24)[0.39] Ma (MSWD = 4.28). This date is interpreted as the eruption and
316 depositional age of the tuff bed.
317 4.3.4 *Salagou Formation (Octon Member)*
318 Zircons were analyzed from four tuff beds spanning over 650 meters of the lower
319 two-thirds of the Octon Member of the Salagou Formation (Fig. 3). Eleven grains were
320 selected from tuff T1 for CA-IDTIMS analysis based on their uniform nature. Of these,
321 eight yielded a concordant and equivalent cluster of isotopic ratios with a weighted mean
322 $^{206}Pb/^{238}U$ date of 284.40 ± 0.07(0.16)[0.34] Ma (MSWD = 0.79), which is interpreted as
323 the eruption and deposition of this tuff. Three grains yielded significantly older ages of
324 285.2 to 290.2 Ma. Tuff bed T2, approximately 40 m higher in the section, produced a
325 number of older inherited grains ranging from 284.8 to 285.4 Ma, as well as a cluster of
326 six equivalent analyses with a weighted mean $^{206}Pb/^{238}U$ date of 284.46 ±
327 0.10(0.17)[0.35] Ma (MSWD = 1.06), interpreted as the age of eruption and deposition.
328 Eight single crystals were dated from tuff bed T9, which was sampled ~300 m
329 above T2. These yielded one significantly older inherited zircon (305 Ma) and a cluster
330 of seven equivalent analyses with a weighted mean $^{206}Pb/^{238}U$ date of 283.53 ±
331 0.10(0.17)[0.34] Ma (MSWD = 1.15), and are interpreted as dating the eruption and
332 deposition of this tuff. Among the fourteen single zircon analyses from tuff bed T12, six
333 yielded Neoproterozoic to Ordovician dates attesting to common inheritance in some
334 zircons from this tuff. Another two analyses yielded dates of 289.8 Ma and are also

interpreted as inherited or recycled from earlier volcanics. Of the remaining six analyses, five yielded equivalent isotope ratios and a weighted mean $^{206}Pb/^{238}U$ date of 282.86 ± 0.13(0.19)[0.35] Ma (MSWD = 1.22) interpreted as the eruption and depositional age of the tuff, while one slightly younger crystal appeared to suffer from a small degree of residual Pb-loss.

5. Discussion5.1 Revised chronostratigraphy

The U-Pb zircon data reported in this study represent the first high-precision CA-IDTIMS ages for interstratified volcanics within the Carboniferous – Permian rift basins of Europe. The resulting precise and accurate ages obtained from the Lodève and Graissessac basins thus have direct consequences for the numerical age of correlated continental sequences throughout eastern Euramerica. These numerical ages also allow the first accurate terrestrial-marine correlation to the late Carboniferous – early Permian global time scale, which has been significantly revised through recent high-precision CA-IDTIMS geochronology (Davydov et al., 2010; Schmitz and Davydov, 2012).

The coal-bearing strata of the basal Graissessac Formation of the western Lodève and eastern Graissessac basins have been previously assigned a biostratigraphic age of Late Stephanian (B+C), or latest Carboniferous, on the basis of abundant and well-preserved paleoflora (Gand et al., 2013 and references therein). The reproducible depositional ages for coal 4 (304.07 ± 0.08 Ma) and coal 5 (303.95 ± 0.07 Ma) tonsteins at Monte Sénégra refine this intercomparison between the continental European and global marine time scales, placing deposition of these strata in the uppermost Kasimovian to lower Gzhelian stages. By comparison the SIMS U-Pb zircon date for the same coal 4

358 tonstein reported by Bruguier et al. (2003) is significantly younger at 295.5 ±5.1 Ma.
359 Unlike chemical abrasion ID-TIMS, the ion probe protocol lacks any grain pre-treatment
360 to remove and mitigate open-system behavior, which can produce anomalously younger
361 ages; thus we interpret the systematics of these ion probe data to be biased by Pb-loss.
362 Other ion probe U-Pb zircon ages of 289 ± 7 Ma and 284 ± 4 Ma for the Viala Formation
363 and Octon Member of the Salagou Formation, respectively (Schneider et al., 2006) are
364 more accurate by comparison with the precise CA-IDTIMS ages obtained in this study
365 for the same units (Table 1). However with a 40 to 80-fold improvement in precision, our
366 ages place much more restrictive constraints on the timing of deposition.
367 A revised chronostratigraphy for the Permian Lodève Basin is presented in Figure
368 2, which also illustrates the CA-IDTIMS zircon ages that pin each formation to the
369 current global time scale (Davydov et al. 2012). When compared with the age chart of
370 Schneider et al. (2006), significant compression of the Lodève record is apparent. Within
371 the first phase of basin development, the shortening of the numerical durations of the
372 Asselian and Sakmarian global stages combined with two volcanic tuff dates restrict
373 significant rock accumulation in the Viala, Tuileres-Loiras, and Usclas St. Privat
374 formations. to late Asselian and Sakmarian time, between ca 296 and 289 Ma. The hiatus
375 at the top of the Viala Formation is constrained to probably less than two million years,
376 before initiation of the second phase of deposition recorded in the overlying Rabejac,
377 Salagou, and La Lieude formations.
378 Four dated tuff beds in the lower Octon Member of the Salagou Formation (Fig.
379 3) span over 650 meters of section (the lower third of the measured succession). The
380 calculated rock accumulation rates for this member are ~0.43 m/ka; extrapolating this rate

381 indicates that the entire 1150 meters of the Octon Member could have been deposited
382 over approximately 2.65 Ma, a much shorter duration than previously interpreted
383 (Schneider et al., 2006; Pochat et al., 2011). Similarly the entire Salagou Formation could
384 have been deposited in approximately 4 Ma under these accumulation rates. However,
385 given the sedimentological distinctions between the Octon and Merifons members., there
386 is the potential for more frequent hiatuses in the latter formation. Therefore, we have
387 been more conservative in our compression of the Salagou Formation, and illustrate it as
388 extending across the Cisuralian-Guadalupian transition, which according to the current
389 geological time scale is constrained numerically at 272 Ma. This stands in stark contrast
390 to earlier interpretations which extended the upper Merifons Member into the
391 Wuchapingian stage.
392 Since the upper Salagou and La Lieude formations lack ashes to produce
393 radioisotopic ages, the only other information available to constrain the minimum age of
394 accumulation in the Lodève Basin is the magnetostratigraphic interpretation of the
395 uppermost sediments of the La Lieude Formation (Evans, 2012; Maillol and Evans,
396 1993). As summarized by Evans (2012), the entire redbed succession of the Lodève
397 Basin is characterized by reverse polarity corresponding to the Kiaman superzone, with
398 the exception of the uppermost sampled bed of the La Lieude Formation, which yielded
399 normal polarity. These data suggest a proximity to the base of the Illawarra mixed
400 polarity interval, which has been constrained in West Texas to near the base of the
401 Capitanian Stage at approximately 265 Ma (Peterson and Nairn, 1971). This constraint is
402 consistent with our previous interpretations for the duration of sediment deposition in the
403 upper Lodève Basin based upon rock accumulation rates. Nonetheless, we might

anticipate additional compression of the absolute duration of Lodève Basin development with additional radioisotope constraints on the poorly calibrated Guadalupian global time scale (Davydov et al., 2012).

The significant changes to the chronostratigraphy of the Lodève Basin, resulting in large part from our new high-precision geochronology, highlight the difficulties in constraining the time scales of terrestrial basin development and associated terrestrial-marine correlations. Several studies have taken the position that lithostratigraphic, biostratigraphic, and proxy climate indicators in assumed contemporaneous European basin records can be correlated into global climate signals (Roscher and Schneider, 2006; Schneider et al., 2006; Tabor and Poulsen, 2008). The extent to which these changes will call the models into question will depend upon further integrative stratigraphic analysis and radioisotope calibration. The correlation of Carboniferous – Permian terrestrial basin records within eastern Euramerica and across Pangaea remains tentative; however further high-precision CA-IDTIMS U-Pb zircon geochronology for other abundant volcanics holds considerable promise for refining the composite stratigraphic record and associated paleoclimate proxy data.

5.2 Paleoclimate Reconstruction

Given the evidence for extensive diagenetic overprinting of Permian strata and paleosols in the Lodève Basin, the typical suite of geochemical proxies (e.g., Sheldon and Tabor, 2009) cannot be applied in a straightforward manner to develop a quantitative mineral- and geochemical-based paleoclimate reconstruction. Nevertheless, many macroscopic paleosol features are notably resistant to diagenetic alteration (Retallack,

427 1991). Furthermore, the range of analogous features among modern soil profiles can help
428 to constrain the range of environmental and climatic conditions when paleosol profiles
429 were undergoing soil formation in the Carboniferous – Permian Lodève Basin.
430 Histosols in modern soil-forming environments are limited to nearly everwet
431 conditions where precipitation exceeds 1000 mm/yr and precipitation exceeds
432 evapotranspiration for at least 10 months each year (Cecil, 2003). Furthermore, slow rates
433 of clastic sedimentation are prerequisite for formation of thick accumulations of organic
434 matter in these types of soils. Therefore, the presence of Histosols in Ghzelian outcrops
435 of the Graissessac Basin and the subsurface of the adjacent Lodève Basin represent
436 relatively humid conditions and intermittently low clastic sedimentation rates during
437 latest Carboniferous time. Furthermore, the presence of contemporaneous Histosol
438 formation in separate basins around the Massif Central suggests a regional climate that
439 was conducive to the accumulation of surficial organic matter and peat accumulation
440 rather than a more local tectonic driver (cf. Pochat and Van den Priessche, 2011). The
441 absence of Histosols in younger Permian strata in the Lodève Basin suggests that climatic
442 conditions dried to the extent that such conditions were no longer conducive to peat
443 formation or that sedimentary accumulation rates increased substantially.
444 The dominant pedogenic process in the formation of Calcisols is the accumulation
445 of carbonate in subsurface soil horizons (Mack et al., 1993). Modern soil profiles that
446 accumulate calcium carbonate in subsurface horizons are most commonly found in
447 climates where evapotranspiration exceeds precipitation for most months of the year
448 (Buol et al., 1997). Specifically, in well-drained soils that receive >760 mm/yr, carbonate
449 will not usually be retained within the subsurface horizons of the soil (Royer, 1999).

Therefore, Calcisols in the Tuilieres-Loiras and the La Lieude formations. are interpreted to represent relatively dry climatic conditions compared to those associated with peat accumulation in the underlying Grasseisac Formation The new $^{206}Pb/^{235}U$ ages presented here from zircon crystals in the mid Tuilleries-Loiras Formation suggests that climatic conditions changed from nearly humid-everwet during the Ghzelian to substantially drier climate by the latest Asselian-earliest Sakmarian in the Lodève Basin.

The dominant pedogenic process in calcic Vertisols is episodic shrink-swell that results from wet-dry cycles as well as accumulation of carbonate (Mack et al., 1993). Shrink-swell processes in Vertisols are commonly a result of the presence of expandable 2:1 clay minerals within the profile that swell during wet periods and contract during dry periods (Buol et al., 1997; Schaetzl and Anderson, 2005; Southard et al., 2012). The expansion and contraction of the profiles leads to characteristic morphological features such as slickensides, pressure faces, clastic dikes, and gilgai surface and mukkara subsurface expression. Additionally, the clotting and presence of many coalescing nucleation sites seen in thin section (Esteban and Klappa, 1983; Fig. 6D) and the presence of wedge-shaped peds with Fe-oxide-stripping and concentration (Fitzpatrick, 1993; Fig. 6F) are attributed to the same shrink-swell processes that created the morphological features described above. These soil types commonly develop in climates characterized by strongly seasonal rainfall such as monsoonal or Mediterranean rainfall patterns (Southard et al., 2012). Not all Vertisols form from seasonal rainfall patterns; some result from episodic fluctuation of the water table (Mintz et al., 2011). However, these groundwater-affected Vertisols also have a characteristic pattern of carbonate formation that transmitted-light and cathodoluminescence petrographic analysis can

identify (Mintz et al. 2011). An Fe/Mn ratio in calcite that favors Mn will is common in vadose zone carbonates and will produce luminescence under cathodoluminence petrography (Hemming et al. 1989). Additionally, presence of dog-tooth spar, microspar and sparry low-mg calcite has been recorded as phreatic environment cements (Esteban and Klappa, 1983; Scholle and Ulmer-Scholle, 2003). Petrographic analysis of carbonate nodules in the calcic Vertisols from the Lodève Basin do not preserve patterns suggestive of groundwater fluctuation. Therefore, calcic Vertisols in the Viala, Rabejac, and parts of the La Lieude formations are interpreted to represent relatively dry climatic conditions during the early Permian characterized by highly seasonal precipitation patterns over the Lodève Basin. Calcic Vertisols in the Sakmarian Viala – Rabejac formations. indicate dry climate, perhaps comparable to those associated with Calcisols in the Asselian – Sakmarian Tuilieres-Loiras Formation, but with a distinct seasonal pattern of rainfall.

The dominant process involved in the creation of vertic Gypsisols is the accumulation of subsurface gypsum in these profiles which indicates substantially drier conditions than during formation of the calcite. These soils are also identified based on the presence of shrink-swell features as described prior. Gypsum is commonly present in subsurface horizons of modern soils that are characterized by evapotrasporation far in excess of precipitation (Eswaran and Zi-Tong, 1991; Watson, 1992). Specifically, gypsum is leached from the soil in regions that receive precipitation in excess of 250 mm/year (Watson 1992). Therefore, vertic Gypsisols in the Merifons Member of the Salagou Formation and the basal La Lieude Formation represent extremely dry conditions in the Artinskian characterized by a seasonal distribution of rainfall and high evapotranspiration rates and relatively low precipitation. Vertic Gypsisols in the

Merifons Member represent continued seasonal precipitation as was present in the Viala – Rabajac based on calcic Vertisols, but with substantially less precipitation or higher rates of evapotranspiration. These conditions are further supported by the presence of illuvial clay coatings and a lack of indicators for pedogenic reducing conditions seen in transmitted light microscopy, which collectively indicate these paleosols formed under exclusively well-drained conditions. Thus, shrink-swell processes did not occur in response to groundwater fluctuations but rather formed in response to regional precipitation patterns. Collectively, paleosol morphologies in the Lodeve Basin define a progressive trend from humid-everwet in latest Carboniferous time to increasingly seasonal and drier climates through the early Permian. The peak in aridity is seen in the Artinskian Merifons Member; however, the presence of Calcicsols and calcic Vertisols in the overlying La Lieude still indicates continued seasonal and dry climates but less arid conditions during the Guadalupian.

6. Implications and Conclusions

The climatic trend observed herein is similar to that observed in other Carboniferous – Permian paratropical basins across Pangaea (Fig. 9). This suggests a regional to global climatic change because all of the basins saw different tectonic controls, and likely different depositional rates, yet all preserve similar stratigraphic trends in climate proxies, which are indicative of the onset of seasonal and relatively arid conditions that persisted from latest Carboniferous through early Permian time. It is unclear if younger Salagou or La Lieude formations preserve middle or upper Permian strata (Fig. 2), but the climate trend preserved in lower Permian succession documented

519 here is remarkably similar to that documented in contemporaneous paratropical basins in
520 western Euramerica (e.g., Cecil, 2003; Eros et al., 2012; Tabor and Montañez, 2002;
521 Tabor and Montañez, 2004).

522 Pochat et al (2011) argued that the depositional history of the Lodève Basin was
523 controlled largely by tectonics, and the resulting changes in sedimentary accommodation
524 under a uniform set of climatic conditions. That model was based on estimated water
525 volume changes of a paleolake that extended across the entire Lodève Basin as the basin
526 infilled and deposition prograded from the southern boundary faults (e.g., Fig. 1). In
527 light of the new chronostratigraphic constraints, and paleosol morphological data
528 presented herein, the model of Pochat and others is not supported for the following
529 reasons:

530 (1) The new chronostratigraphic dates limit the majority of the Lodève Basin
531 Permian strata to the lower Permian. Prior to this work much of the Salagou Formation
532 was thought to be deposited from Kungurian to Wuchiapingian time. It is now known
533 that most of the Salagou Formation is limited to the Sakmarian. Therefore, the temporal
534 evolution of lake volumes and sedimentary rates in the Lodève Basin discussed by Pochat
535 and others (2011) are no longer valid.

536 (2) The presence of paleosols throughout the Lodève Basin sedimentary record is
537 definitive evidence that the entire basin was not always filled by a large lake. The
538 presence of Histosols in the Carboniferous succession indicate poorly-drained conditions
539 and high levels of a regional water table. However, pedogenic carbonate, illuviated clays,
540 and gypsum in subsurface horizons of Permian paleosols indicate a relative fall in the
541 regional water table and well-drained conditions that were distal from any lake body, that

might have been present in the Lodève Basin. As a result, the water volume changes in the Lodève Basin discussed by Pochat and Van den Priessche (2011) were overestimated by their model.

(3) While Pochat and Van Den Driessche (2011) are correct that this basin fits the model of a quadripartite continental-rift sequence controlled by tectonics, this basin preserves a record of climate indicators and paleoclimatic change that agrees with other paratropical basins that did not evolve under the same tectonic regimes (e.g., Tabor and Montañez, 2004; Tabor et al., 2008; Bishop et al., 2010). Therefore, while tectonics may have affected depositional style in the Lodève Basin, there are clearly extrabasinal mechanisms such as long-term aridification and increasing seasonality that affected the long-term history of sedimentation in the basin. A megafan sequence stratigraphic model for continental sedimentary basins suggests a common evolution of sedimentary infill that evolves from initially poorly-drained conditions to progressively better drained conditions through time (Weissmann et al., 2013). At first glance, the Lodève Basin fits this model in that the paleosols change from poorly drained Histosols in the Ghezlian to well-drained vertic Gypisols, calcic Vertisols, and Calcisols in younger Permian strata. However, considering this model under a uniform set of climatic conditions, the poorly-drained Carboniferous Histosols that required ever-wet conditions, would likely have given way to well-drained argillisols/Oxisols in Permian strata under a similarly humid climate. Moreover, the well-drained paleosols seen in the Permian would likely have corresponding poorly-drained gypsic Gleysols and calcic Gleysols in the Carboniferous strata under a uniform semi-arid climate. Note that neither one of these conditions accommodate the evidence for seasonal precipitation that is a prerequisite for Vertisol

565 formation. Additionally, the presence of similar trends in penecontemporaeous low-
566 latitude Carboniferous – Permian basins under different types of tectonic controls,
567 suggests a large-scale regional to global mechanism that is explained most
568 parsimoniously by climate change. Therefore, we conclude that long-term pan-tropical
569 climate change was a dominant factor in the evolution of Lodève Basin sedimentary
570 infill.
571
572 **Acknowledgements** We would like to thank Prof. Finn Surlyk, Greg Ludvigson and an
573 anonymous reviewer for their revisions and suggestions on this manuscript. We thank
574 Erik Gulbranson, Mike Eros, Jörg W. Schneider, and Frank Körner for help and
575 assistance in the field. This research was funded by National Science Foundation (NSF
576 EAR0545654 to NJT and IPM), the Geological Society of America, the University of
577 California at Davis, and Southern Methodist University. VID was partially funded
578 through the Russian Government Program of Competitive Growth of Kazan Federal
579 University.
580 **References**

581 Beauchamp, B., 1994. Permian climatic cooling in the Canadian Arctic. Geological
582 Society of America Special Paper 288, 229 – 246.
583 Bishop, J.W., Montañez, I.P., Osleger, D.A., 2010. Dynamic Carboniferous climate
584 change, Arrow Canyon, Nevada. Geosphere 6, 1 – 34.
585 Blackwell, D.D., 1971. The Thermal Structure of the Continental Crust. In: Heacock, J.G.
586 (Ed.), The Structure and Physical Properties of the Earth's Crust. Geophysical
587 Monograph, pp. 169 – 184.
588 Breitkreuz, C., Kennedy, A., 1999. Magmatic flare-up at the Carboniferous/Permian
589 boundary in the NE German Basin revealed by SHRIMP zircon ages.
590 Tectonophysics 302, 307 – 326.
591 Bruguier, O., Becq-Giraudon, J.-F., Champenois, M., Deloule, E., Ludden, J., Mangin,
592 D., 2003. Application of in situ zircon geochronology and accessory phase
593 chemistry to constraining basin development during post-collisional extension: a
594 case study from the French Massif Central. Chemical Geology 201, 319 – 336.

595 Buatier, M.D., Deneele, D., Dubois, M., Potdevin, J.-L., Lopez, M., 2000. Nacrite in the
596 Lodeve Basin: a TEM and fluid-inclusion study. European Journal of Mineralogy
597 12,. 329 – 340.
598 Bullock, P., Fédoroff, N., Jungerius, A., Stoops, G., Tursina, T., Babel, U., 1985.
599 Handbook for Soil Thin Section Description. Waine Research Publications,
600 Wolverhampton, UK, 152 p.
601 Buol, S.W., Southard, R.J., Graham, R.C., McDaniel, P.A., 1997. Soil Genesis and
602 Classification: 4th ed. Iowa State University Press, Ames, IA, 527 p.
603 Burger, K., Hess, J.C., Lippolt, H.J., 1997. Tephrochronologie mit Kaolin-
604 Kohlentonsteinen: mittel zur Korrelation paralischer und limnischer ablagerungen
605 des Oberkarbons. Geologisches Jahrbuch A 147, 3 – 39.
606 Cecil, C.B., 1990. Paleoclimate controls of stratigraphic repetion of chemical and
607 siliciclastic rocks. Geology 18, 533 – 536.
608 Cecil, C.B., 2003. The Concept of Autocyclic and Allocyclic Controls on Sedimentation
609 and Stratigraphy, Emphasizing the Climatic Variable. In Cecil, C.B., Edgar, N.T.
610 (Eds.), Climate Controls on Stratigraphy. SEPM Special Publication 77, 13 – 20.
611 Cecil, C.B., Dulong, F.T., West, R.R., Stamm, R., Wardlaw, B., Edgar, N.T., 2003.
612 Climate controls on the stratigraphy of a middle Pennsylvanian cyclothem in
613 North America. In: Cecil, C.B., Edgar, N.T.(Eds.), Climate Controls on
614 Stratigraphy. SEPM Special Publication 77, pp. 151 – 180.
615 Chen, Y., Faure, M., Cogné, J.P., 1997. Late Permian palaeomagnetic results from the
616 Brive basin (Massif Central, France). Tectonophysics, 281, 209 – 220.
617 Cogné, J.P., Brun, J.P., Van Den Driessche, J., 1990. Paleomagnetic evidence for rotation
618 during Stephano-Permian extension in southern Massif Central (France). Earth
619 and Planetary Science Letters 101, 272 – 280.
620 Condie, K.C., 1997. Plate Teconics and Crustal Evolution.4th ed. Heinemann-
621 Butterworth, Oxford, 282 p.
622 Condon, D., Schoene, B., Bowring, S., Parrish, R., McLean, N., Noble, S., Crowley, Q.,
623 2007. EARTHTIME: isotopic tracers and optimized solutions for high-precision
624 U-Pb ID-TIMS geochronology. Eos (Transactions, American Geophysical Union)
625 88, abs. V41E-06.
626 Conrad, G., Odin, B., 1984. Le Bassin Permien de Lodeve (Herault), Livret-guide de
627 l'excursion. Laboratoire de Sedimentologie. Universite d'Aix, Congrese European
628 de Sedimentologie a Marseille, Universite d'Aix-Marseille, 59 p.
629 Copard, Y., Disnar, J.R., Becq-Giraudon, J.-F., Boussafir, M., 2000. Evidence and effects
630 of fluid circulation on organic matter in intramontane coalfields (Massif Central,
631 France). Interational Journal of Coal Geology44, 49 – 68.
632 Davydov, V.I., Crowley, J.L., Schmitz, M.D., Poletaev, V.I., 2010. High-precision U-Pb
633 zircon age calibration of the global Carboniferous time-scale and Milankovitch-
634 band cyclicity in the Donets Basin, eastern Ukraine. Geochemistry, Geophysics,
635 Geosystems 11, doi://10.1029/2009GC002736..
636 Davydov, V.I., Korn, D., Schmitz, M.D., 2012. The Carboniferous Period, in: Gradstein,
637 F.M., Ogg, J.G., Schmitz, M.D., Ogg, G.M. (Eds.), The Geological Time Scale
638 2012. Elsevier, pp. 603 – 652.

Davydov, V.I., Wardlaw, B.R., Gradstein, F.M., 2004. The Carboniferous Period, in: Gradstein, F.M., Ogg, J.G., Smith, A.G.(Eds.), A Geological Time Scale 2004. Cambridge University Press, Cambridge, pp. 222 – 248.

Diego-Orozco, A., Henry, B., 1993. Paleomagnetic results from the Permian Saint-Affrique basin (France) and implications for late and post-Hercynian tectonics. Tectonophysics 227, 31 – 47.

DiMichele, W.A., 2014. Wetland-dryland vegetational dynamics in Pennsylvanian ice age tropics. International Journal of Plant Sciences 175, 123 – 164.

DiMichele, W.A., Tabor, N.J., Chaney, D.S., Nelson, W.J., 2006. From wetlands to wet spots: Environmental tracking and the fate of Carboniferous elements in Early Permian tropical floras, in Greb, S.F. DiMichele, W.A. (Eds.), Wetlands Through Time: Geological Society of America Special Paper 399, pp. 223 – 248.

Eros, J.M., Montañez, I.P., Osleger, D.A., Davydov, V.I., Nemyrovska, T.I., Poletaev, V.I., Zhykalyak, M.V., 2012. Sequence stratigraphy and onlap history of the Donets Basin, Ukraine: Insight into Carboniferous icehouse dynamics. Palaeogeography, Palaeoclimatology, Palaeoecology 313-314, 1 – 25.

Esteban, M., Klappa, C.F., 1983. Subaerial Exposure Environment, in Scholle, P.A., Bebout, D.G., Moores, C.H., (Eds.), Carbonate Depositional Environments. American Association of Petroleum Geologists Memoir 33, 1 – 96.

Eswaran, H., Zi-Tong, G., 1991. Properties, Genesis, Classification, and Distribution of Soils with Gypsum. Occurrence, Characeristics, and Genesis of Carbonate, Gypsum, and Silica Accumulations in Soils, SSSA Special Publication 26, 89 – 119.

Evans, M.E., 2012. Magnetostratigraphy of the Lodéve Basin, France: Implications for the Permo-Carboniferous reversed superchron and the geocentric axial diple. Studia Geophysica et Geodaetica 56, 725 – 734.

Falcon-Lang, H.J., 2000. Fire ecology of the Carboniferous tropical zone. Palaeogeography, Palaeoclimatology, Palaeoecology 164, 339 – 355.

Falcon-Lang, H.J., Benton, M.J., Braddy, S.J., Davis, S.J., 2006. The Pennsylvanian tropical biome reconstructed from the Joggins Formation of Nova Scotia, Canada. Journal of the Geological Society, London 163, 561 – 576.

Gand, G., Galtier, J., Garric, J., Teboul, P.-A., Pellenard, P., 2013. Discovery of an Autunian macroflora and lithostratigraphic re-investigation on the western border of the Lodéve Permian basin (Mont Sénégra, Hérault, France). Paleoenvironmental implications. Comptes Rendus Palevol 12, 69 – 79.

Gand, G., Lapeyrie, J., Garric, J., Nel, A., Schneider, J., Walter, H., 1997. Découverte d'Arthropodes et de bivalves inédits dans le Permien continental (Lodévois, France). Comptes Rendus de l'Académie des Sciences - Series IIA - Earth and Planetary Science 325, 891 – 898.

Gastaldo, R.A., Purkynová, E., Zbynek, S., Schmitz, M.D., 2009. Ecological Persistence in the Late Mississippian (Serpukhovian, Namurian A) Megafloral Record of the Upper Silesian Basin, Czech Republic. Palaios 24,: 336 – 350.

Goll, M., Lippold, H.J., 2001. Biotit-Geochronologie ($^{40}Ar_{rad}/K$, $^{40}Ar_{rad}/^{39}Ar_K$, $^{87}Sr_{rad}/^{87}Rb$) spat-variszischer Magmatite des Thuringer Waldes. N. Jahrbuch Geol. Paläontol 222, 353 – 405.

684 Gradstein, F.M., Ogg, J.G., Smith, A.G., 2004. A Geological Time Scale: 2004.
685 Cambridge University Press, Cambridge, U.K.
686 Gulbranson, E.L., Montañez, I.P., Schmitz, M.D., Limarino, C.O., J.L., I., Marenssi,
687 S.A., Crowley, J.L., 2010. High-precision U-Pb calibration of Carboniferous
688 glaciation and climate history, Paganzo Group, NW Argentina. Geological
689 Society of America Bulletin 122, 1480 – 1498.
690 Gulbranson, E.L., Montañez, I.P., Tabor, N.J., Limarino, C.O., in press. Late
691 Pennslyvanian aridification on the southwestern margin of Gondwana (Paganzo
692 Basin, NW Argentina): A regional expression of a global climate perturbation.
693 Palaeogeography, Palaeoclimatology, Palaeoecology
694 doi:10.1016/j.palaeo.2014.10.029.
695 Hanson, R.F., Zamora, R., Keller, W.D., 1981. Nacrite, Dickite, and Kaolinite in One
696 Deposit in Nayarit, Mexico. Clay and Clay Minerals 29, 451 – 453.
697 Harris, N.B., Freeman, K.H., Pancost, R.D., White, T.S., Mitchell, G.D., 2004. The
698 character and origin of lacustrine source rocks in the Lower Cretaceous synrift
699 section, Congo Basin, west Africa. American Association of Petroleum
700 Geologists Bulletin 88,: 1163 – 1184.
701 Hemming, N.G., Meyers, W.J., Grams, J.C., 1989. Cathodoluminescence in Diagenetic
702 Calcites: The Role of Fe and Mn as Deduced from Electron Probe and
703 Spectrophotometric Measurements.Journal of Sedimentary Petrology 59, 404 –
704 411.
705 Henderson, C.M., Davydov, V.I., Wardlaw, B.R., 2012. The Permian Period, in:
706 Gradstein, F.M., Ogg, J.G., Schmitz, M.D., Ogg, G.M. (Eds.), The Geological
707 Time Scale 2012. Elsevier, pp. 653 – 680.
708 Henry, B., Becq-Giraudon, J.-F., Rouvier, H., 1999. Palaeomagnetic studies in the
709 Permian Basin of Largentiere and implications for the Late Variscan rotations in
710 the French Massif Central. Geophysics Journal International 138, 188 – 198.
711 Hess, J.C., Lippolt, H.J., 1986. $^{40}Ar/^{39}Ar$ ages of tonstein and tuff sanidines: New
712 calibration points for the imporvement of the Upper Carboniferous time scale.
713 Chemical Geology 59, 143 – 154.
714 Jaffey, A.H., Flynn, K.F., Glendenin, L.E., Bentley, W.C., A.M., E., 1971. Precision
715 measurements of half-lives and specific activities of ^{235}U and ^{238}U. Physical
716 Review C 4, 1889 – 1906.
717 Kahmann, J.A., Driese, S.G., 2008. Paleopedology and geochemistry of Late
718 Mississippian (Chesterian) Pennington Formation paleosols at Pound Gap,
719 Kentucky, USA: Implications for high-frequency climate variations.
720 Palaeogeography, Palaeoclimatology, Palaeoecology 259, 357 – 381.
721 Königer, S., Lorenz, V., Stollhofen, H., Armstrong, R., 2002. Origin, age, and
722 stratigraphic significance of distal fallout ash tuffs from the Carboniferous-
723 Permian continental Saar-Nahe Basin (SW Germany). International Journal of
724 Earth Sciences 91, 341 – 356.
725 Körner, F., Schneider, J.W., Gand, G., 2005. Sedimentology and geochemistry of the
726 Permian red beds of the Lodéve Basin - implications for environment and climate,
727 Abstracts Permian and Triassic playas Symposium, Montpellier, pp. 17 – 18.

728 Körner, F., Schneider, J.W., Hoernes, S., Gand, G., Kleeberg, R., 2003. Climate and
729 continental sedimentation in the Permian of the Lodeve Basin (Southern France).
730 Bollettino della Societa Geologica Italiana. Volume specialeno. 2, 185 – 119.
731 Lambiase, J.J., 1990. A model for tectonic control of lacustrine stratigraphic sequences in
732 continental rift basins, in: Katz, B.J.(Ed.), Lacustrine Exploration: Case Studies
733 and Modern Analogues. AAPG Memoir, pp. 265 – 276.
734 Lefournier, J., 1980. Dépôts de pré-ouverture de l'Atlantique Sud. Comparaison avec la
735 sédimentation actuelle dans la branche occidentale des Rifts Est-Africain.
736 Recharche géologique en Afrique 5, 127 – 130.
737 Limarino, C.O., Cesari, S., N., Spalletti, L.A., Taboada, A.C., Isbell, J.L., Geuna, S.,
738 Gulbranson, E.L., 2014. A paleoclimatic review of southern South America
739 during the late Paleozoic: A record from icehouse to extreme greenhouse
740 conditions. Gondwana Research 25, 1396 – 1421.
741 Machette, M.N., 1985. Calcic soils of the southwestern United States, in: Weide, D.L.,
742 Faber, M.L. (Eds.), Soils and Quaternary Geology of the Southwestern United
743 States. Geological Society of America, pp. 1 – 21.
744 Mack, G.H., James, W.C., Monger, H.C., 1993. Classification of paleosols. Geological
745 Society of America Bulletin 105,. 129 – 136.
746 Maillol, J.-M., Evans, M.E., 1993. Permian palaeosecular variation as recorded in the
747 Lodéve redbeds, southern France. Geologica Carpathica 44, 281 – 287.
748 Mattinson, J.M., 2005. Zircon U-Pb chemical abrasion ("CA-TIMS") method: combined
749 annealing and multi-step partial dissolution analysis for improved precision and
750 accuracy of zircon ages. Chemical Geology 220, 47 – 66.
751 Mintz, J.S., Driese, S.G., Breecker, D.O., Ludvigson, G.A., 2011. Influence of Changing
752 Hydrology on Pedogenic Calcite Precipitation in Vertisols, Dance Bayou,
753 Brazoria County Texas, U.S.A.: Implications for Estimating Paleoatmospheric
754 pCO_2. Journal of Sedimentary Research 81, 394 – 400.
755 Montañez, I.P., Tabor, N.J., Niemeier, D., DiMichele, W.A., Frank, T.D., Fielding, C.R.,
756 Isbell, J.L., Birgenheier, L.P., Rygel, M.C., 2007. CO_2-Forced Climate and
757 Vegetation Instability During Late Paleozoic Deglaciation. Science 315, 87 – 91.
758 Peterson, D.N., Nairn, A.E.M., 1971. Palaeomagnetism of Permian redbeds from the
759 South-western United States. Geophysical Journal of the Royal Astronomical
760 Society 23, 191 – 205.
761 Peyser, C.E., Poulsen, C.J., 2008. Controls on Permo-Carboniferous Precipitation over
762 Tropical Pangaea: A GCM sensitivity study. Palaeogeography,
763 Palaeoclimatology, Palaeoecology 268, 181 – 192.
764 Pochat, S., Van Den Driessche, J., 2011. Filling sequence in Late Paleozoic continental
765 basins: A chimera of climate change? A new light shed given by the Graissessac -
766 Lodéve basin (SE France). Palaeogeography, Palaeoclimatology, Palaeoecology
767 302, 170 – 186.
768 Pochat, S., Van Den Driessche, J., Mouton, V., Guillocheau, F., 2005. Identification of
769 Permian palaeowind direction from wave-dominated lacustrine sediments
770 (Lodeve Basin, France). Sedimentology 52, 809 – 825.
771 Prosser, S., 1993. Rift-related linked depositional systems and their seismic expression,
772 in: Williams, G.D., Dobb, A. (Eds.), Tectonics and Sesimic Sequence
773 Stratigraphy. Geological Society of London, Special Publication 71, pp. 35 – 66.

774 Quast, A., Hoefs, J., Paul, J., 2006. Pedogenic carbonates as a proxy for palaeo-CO_2 in
775 the Palaeozoic atmosphere. Palaeogeography, Palaeoclimatology, Palaeoecology
776 242, 110 – 125.
777 Retallack, G.J., 1988. Field recognition of paleosols, in: Reinhardt, J., Sigleo, W.R.
778 (Eds.), Paleosols and weathering through geologic time: principles and
779 applications. Special Paper of the Geological Society of America 216, pp. 1 – 20.
780 Retallack, G.J., 1991. Untangling the Effects of Burial Alteration and Ancient Soil
781 Formation. Annual Review of Earth and Planetary Sciences 19, 183 – 206.
782 Roscher, M., Schneider, J.W., 2006. Permo-Carboniferous climate: Early Pennsylvanian
783 to Late Permian climate development of central Europe in a regional and global
784 context. Geological Society of London, Special Publication 265, 95 – 136.
785 Rosenau, N.A., Tabor, N.J., Elrick, S.D., Nelson, W.J., 2013a. Polygenetic History of
786 Paleosols In Middle-Upper Pennslyvanian Cyclothems of the Illinois Basin,
787 U.S.A.: Part I. Characterization of Paleosol Types and Interpretation of Pedogenic
788 Processes. Journal of Sedimentary Research 83, 606 – 636.
789 Rosenau, N.A., Tabor, N.J., Elrick, S.D., Nelson, W.J., 2013b. Polygenetic History of
790 Paleosols in Middle-Upper Pennsylvanian Cyclothems of the Illinois Basin,
791 U.S.A.: Part II. Integrating Geomorphology, Climate, and Glacioeustasy. Journal
792 of Sedimentary Research 83, 637 – 668.
793 Royer, D.L., 1999. Depth to pedogenic carbonate horizon as a paleoprecipitation
794 indicator? Geology 27, 1123 – 1126.
795 Royer, D.L., Berner, R.A., Montañez, I.P., Tabor, N.J., Beerling, D.J., 2004. CO_2 as a
796 primary driver of Phanerozoic climate. GSA Today 14, 4 – 10.
797 Schaetzl, R.J., Anderson, S. (Eds.), 2005. Soils: Genesis and Geomorphology. Cambridge
798 University Press, p. 827.
799 Schlische, R.W., 1991. Half-graben basin filling models: New constraints on continental
800 extensional basin evolution. Basin Research 3, 123 – 141.
801 Schmitz, M.D., Davydov, V.I., 2012. Quantitative radiometric and biostratigraphic
802 calibration of the global Pennsylvanian - Early Permian time scale. Geological
803 Society of America Bulletin 124, 549 – 577.
804 Schmitz, M.D., Schoene, B., 2007. Derivation of isotope ratios, errors and error
805 correlations for U-Pb geochronology using ^{205}Pb - ^{235}U- (^{233}U)-spiked isotope
806 dilution thermal ionization mass spectrometric data. Geochemistry, Geophysics,
807 Geosystems 8, doi:10.1029/2006GC001492.
808 Schneider, J.W., Körner, F., Roscher, M., Kroner, U., 2006. Permian climate
809 development in the northern peri-Tethys area - The Lodeve basin, French Massif
810 Central, compared in a European and global context. Palaeogeography,
811 Palaeoclimatology, Palaeoecology 240, 161 – 183.
812 Schoeneberger, P.J., Wysocki, D.A., Benham, E.C., Soil Science Staff, 2012. Field book
813 for describing and sampling soils, version 3.0. Natural Resources Conservation
814 Service, National Soil Survey Center, Lincoln, NE.
815 Scholle, P.A., Ulmer-Scholle, D.S., 2003. A Color Guide to the Petrography of Carbonate
816 Rocks: Grains, Textures, Porosity, Diagensis. American Association of Petroleum
817 Geologists Memoir 77, 474 p.
818 Sheldon, N.D., Tabor, N.J., 2009. Quantitative paleoenvironmental and paleoclimatic
819 reconstruction using paleosols. Earth-Science Reviews 95, 1 – 52.

820 Shen, Z.Y., Wilson, M.J., Fraser, A.R., Pearson, M.J., 1994. Nacritic Clay Associated
821 with the Jiangshan-Shaoxing Deep Fault in Zhejiang Province, China. Clay and
822 Clay Minerals 42, 576 – 581.
823 Southard, R.J., Driese, S.G., Nordt, L.C., 2012. Vertisols, in: Huang, P.M., Li, Y.,
824 Sumner, M.E. (Eds.), Handbook of Soil Science. 2nd Edition ed. CRC Press, Boca
825 Raton, Florida, pp. 33-82 – 33-97.
826 Stoops, G., 2003. Guidelines for Analysis and Description of Soil and Regolith Thin
827 Sections. Soil Science Society of America, Madison, WI.
828 Stoops, G., Marcelino, V., Mees, F., 2010. Interpretation of Micromorphological Features
829 of Soils and Regoliths. Elsevier, New York, NY.
830 Tabor, N.J., Montañez, I.P., 2002. Shifts in late Paleozoic atmospheric circulation over
831 western equatorial Pangea: Insights from pedogenic mineral $\delta^{18}O$ compositions.
832 Geology 30, 1127 – 1130.
833 Tabor, N.J., Montañez, I.P., 2004. Morphology and distribution of fossil soils in the
834 Permo-Pennsylvanian Witchita and Bowie Groups, north-central Texas, USA:
835 implications for western equatorial Pangean palaeoclimate during icehouse-
836 greenhouse transition. Sedimentology 51, 851 – 884.
837 Tabor, N.J., Montañez, I.P., Kelso, K.A., Currie, B., Shipman, T., Colombi, C., 2006. A
838 Late Triassic soil catena: Landscape and climate controls on paleosol morphology
839 and chemistry across the Carnian-age Ischigualasto-Villa Union basin,
840 northwestern Argentina. Geological Society of America Special Paper 416, 17 –
841 41.
842 Tabor, N.J., Montañez, I.P., Scotese, C.R., Poulsen, C.J., Mack, G.H., 2008. Paleosol
843 Archives of Environmental and Climatic History in paleotropical Western
844 Euramerica during the latest Pennsylvanian through Early Permian. Geological
845 Society of America Special Volume 441, 291 – 304.
846 Tabor, N.J., Montañez, I.P., Zierenberg, R., Currie, B.S., 2004. Mineralogical and
847 geochemical evolution of a basalt-hosted fossil soil (Late Triassic, Ischigualasto
848 Formation, northwest Argentina): Potential for paleoenvironmental reconstructon.
849 GSA Bulletin 116, 1280 – 1293.
850 Tabor, N.J., Myers, T.S., Gulbranson, E., Rasmussen, C., Sheldon, N.D., 2013. Carbon
851 Stable Isotope Composition of Modern Calcareous Soil Profiles in California:
852 Implications for CO_2 Reconstructions from Calcareous Paleosols, in: Driese, S.D.,
853 Nordt, L.C. (Eds.), New Frontiers in Paleopedology and Terrestrial
854 Paleoclimatology: Paleosols and Soil Surface Analog Systems. SEPM Special
855 Publication 104, pp. 17 – 34.
856 Tabor, N.J., Poulsen, C.J., 2008. Palaeoclimate across the Late Pennsylvanian-Early
857 Permian tropical palaeolatitudes: A review of climate indicators, their
858 distribution, and relation to palaeophysiographic climate factors.
859 Palaeogeography, Palaeoclimatology, Palaeoecology 268, 293 – 310.
860 Thomas, S.G., Tabor, N.J., Yang, W., Myers, T.S., Yang, Y., Wang, D., 2011. Palaeosol
861 stratigraphy across the Permian-Triassic boundary, Bogda Mountains, NW China:
862 Implications for palaeoenvironmental transition through earth's largest mass
863 extinction. Palaeogeography, Palaeoclimatology, Palaeoecology 308, 41 – 64.

Von Der Borch, C.C., Bolton, B., Warren, J.K., 1977. Environmental setting and microstructure of subfossil lithified stromatolites associated with evaporites, Marion Lake, South Australia. Sedimentology 24, 693 – 708.

Wardlaw, B.R., Davydov, V.I., Gradstein, F.M., 2004. The Permian Period, in: Gradstein, F.M., Ogg, J.G., Smith, A.G. (Eds.), A Geologic Time Scale 2004. Cambridge University Press, Cambridge, pp. 249 – 270.

Watson, A., 1992. Desert Soils, in: Martini, I.P., Chesworth, W. (Eds.), Weathering, Soils & Paleosols. Developments in Earth Surface Processes 2. Elsevier, New York, pp. 225-260.

Weissmann, G.S., Hartley, A.J., Scuderi, L.A., Nichols, G.J., Davidson, S.K., Owen, A., Atchley, S.C., Bhattacharya, P., Chakraborty, T., Ghosh, P., Nordt, L.C., Michel, L.A., Tabor, N.J., 2013. Prograding Distributive Fluvial Systems - Geomorphic Models and Ancient Examples, in: Driese, S.D., and Nordt, L.C. (Eds.), New Frontiers in Paleopedology and Terrestrial Paleoclimatology: Paleosols and Soil Surface Analog Systems, SEPM Special Publication 104, 131 – 147.

Ziegler, A.M., Hulver, M.L., Rowley, D.B., 1997. Permian world topography and climate, in: Martini, I.P. (Ed.), Late Glacial and Post-Glacial Environmental Changes - Quaternary, Carboniferous-Permian and Proterozoic. Oxford University Press, Oxford, pp. 111 – 146.

FIGURE CAPTIONS

Fig. 1 Graissessac and Lodève basins: A) Inset location map showing position of the Graissessac and Lodève basins (star) within the French Massif Central (outlined in black); B) outcrop area of the Graissessac and Lodève basins; C) geologic map of the Lodève Basin, modified from Schneider and others (2006), with the locations of sampling sites (red stars) studied herein. Solid black lines represent roads, while dashed lines are major basin-bounding faults. The Saxonien formations include (in ascending order) the Rabajac Formation, Octon and Merifons Members of the Salagou Formation, and La Lieude Formation

Fig. 2 Generalized stratigraphic column for the Graissessac and Lodève basins (adapted from Schneider et al. 2006 and references therein). Chronostratigraphy and age scale on left is based on biostratigraphic correlation using fossil cockroach wings collected in the Lodève Basin (Schneider et al., 2006) compiled with the time scale calibration of GTS 2004 (Davydov et al., 2004; Wardlaw et al., 2004). A revised chronostratigraphy, on the

right of the diagram, is based upon ID-TIMS high-precision U-Pb ages presented here, tied to the GTS 2012 time-scale (Davydov et al., 2012; Henderson et al., 2012). Red lines represent locations of ashes sampled in this study.

Fig. 3 Detailed stratigraphic column of the Permian siliclastic succession that crop out in the Lodève Basin (adapted from Schneider et al 2006). Roman numerals and T#s are tuff horizons described in previous studies (Gand et al., 1997; Körner et al., 2005). The stratigraphic occurrence of paleosol morphologies are marked in the right column and correspond to the morphologies presented in Figure 5: C = Calcisols, CV = calcic Vertisols, and VG = vertic Gypsisols. Yellow tuffs represent ashes sampled and data presented herein.

Fig. 4 Pedotypes found within the strata of the Lodeve Basin. Orange dendtritic texture marks the occurrence of jarosite. Arcuate lines represent the occurence of slickensides. White ovals are carbonate nodules, while Ts are indurate carbonate horizons. The thin fenestral black lines denote the prior occurence of pedogenic gypsum (now satin spar calcite).

Fig. 5 Examples of pedogenic features seen in the field. (A) Intercalated coal seams, ashes, and siliciclastics characteristic of the Graissessac Formation (B) Groundwater carbonate nodule. (C) Pedogenic carbonate nodules and slickensides in a vertic Calcisol. Scale is ~2 m from base of section to outcrop. (D) Clastic dikes infilled by sandstone in a vertic Calcisol. (E) Close up of the top of a vertic Gypsisol. Note desiccation cracks on the upper surface of paleosol. (F) Stacked vertic Gypsisols of the Merifons Member, Salagou Formation Green layers are the surface.

Fig. 6 Examples of pedogenic features in thin section. All images were taken under 1.25x magnification. (A) Orabated mite fecal material, (B) Boxwork fabric was originally micritic calcite and is now altered to microspar and dolomite. (C) Brown areas are roots seen both in axial and longitudinal view. Note the longitudinal root has been dissected probably as a result of shrink-swell processes. Also seen is a root halo (white area encompassing part of the root). (D) Clotted micrite texture of a rhizolith encircling Fe-Mn infilled root chamber. (E) Hematite replacing primary clay. (F) Wedge-shaped peds.

Fig. 7 U-Pb concordia diagrams illustrating single zircon isotopic analyses for dated tonstein and tuff beds of the Graissessac and Lodeve basins. All error ellipses are plotted at the 2σ confidence interval. Weighted mean $^{206}Pb/^{238}U$ dates and uncertainties (95% confidence interval) are indicated for the clusters of analyses (shaded) interpreted to represent the magmatic populations; analyses with open symbols were excluded from the weighted mean calculations (see Results section for discussion).

Fig. 8 Paleoclimate reconstruction adapted from Tabor and Poulsen (2008) for western and central equatorial Pangea including Lodève Basin. International geological time-scale according to Gradstein et al. (2004), while basin trends have been updated using the dates from Montanez and others (2007) and those presented herein. Climate trends (with paleo-latitudes indicated) are based on observed climate-sensitive facies as presented in Tabor and Poulsen 2008. "Wet" indicates the presence of climate-sensitive facies corresponding to ever-wet or humid conditions (>1000 mm/yr) and PPT>ETV for at least 9 months, including coals, laterites. "Dry" indicates the presence of climate-sensitive facies corresponding to semi-arid and arid conditions where precipitation is less that ~760 mm/yr and fewer than 5 months/yr with precipitation in excess of evapotranspiration

(Cecil et al., 2003). Orange shading denotes intervals with evidence of distinct seasonality including vertic paleosol morphology (e.g. Kahmann and Driese, 2008; Tabor and Montañez, 2004) and fusain (Falcon-Lang, 2000; Falcon-Lang et al., 2006). The schematic climate surveys are constructed from high-resolution, intrabasinal studies of paleoclimate indicators cited throughout the text and references cited therein.

Figures

Figure 1

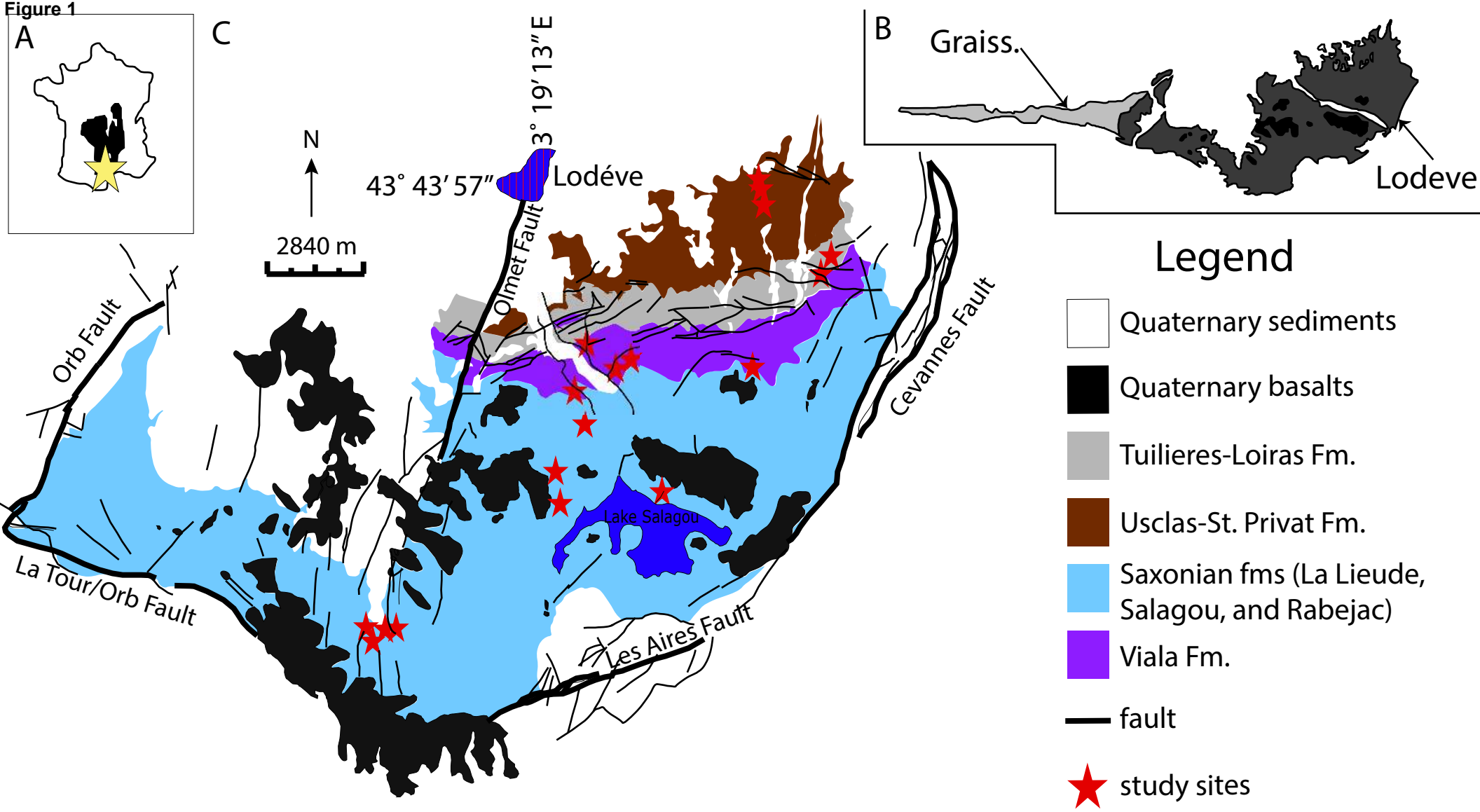

Figure 2

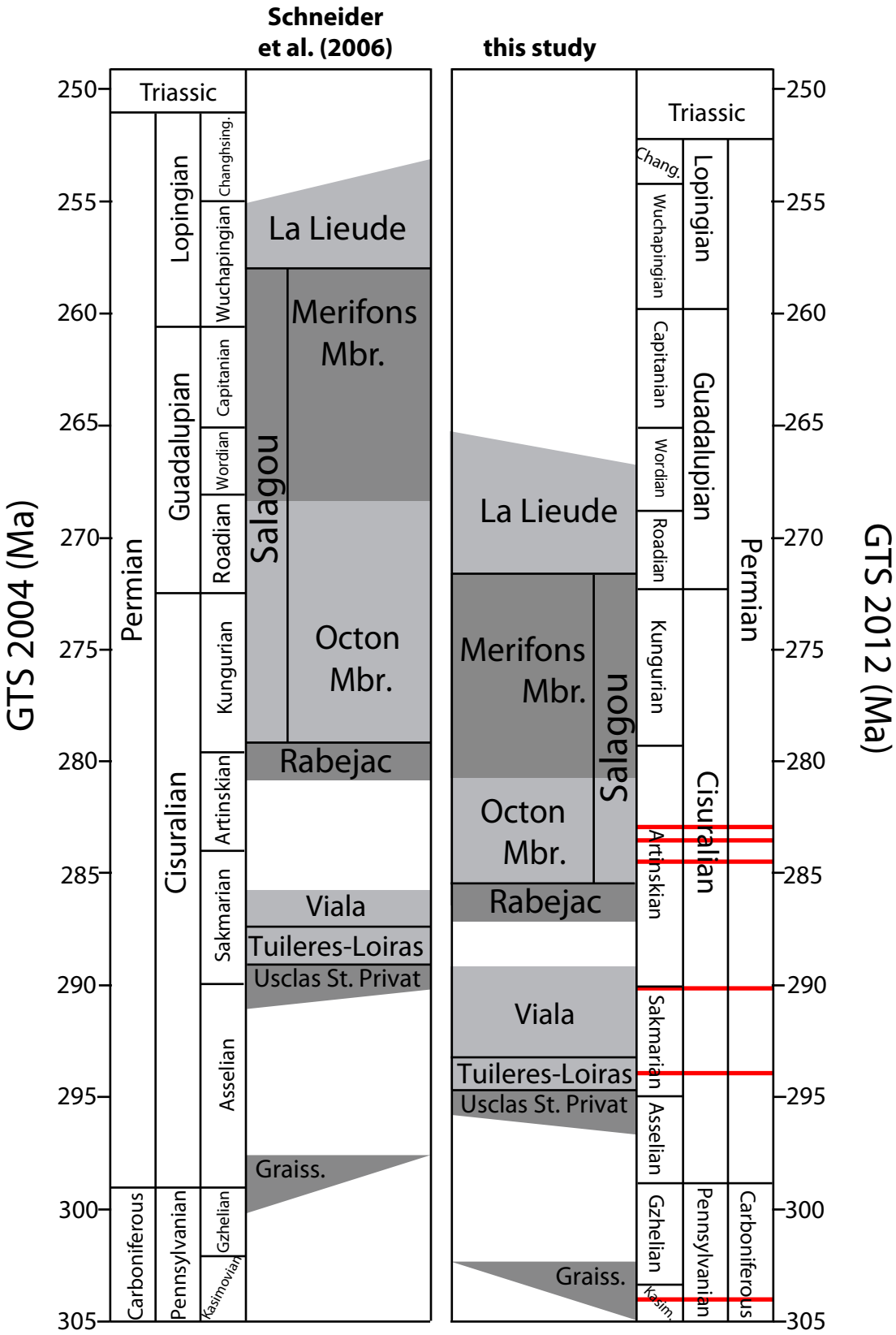
Schneider et al. (2006)
this study
GTS 2004 (Ma)
GTS 2012 (Ma)
250
255
260
265
270
275
280
285
290
295
300
305
Triassic
Permian
Carboniferous
Pennsylvanian
Lopingian
Guadalupian
Cisuralian
Changhsing.
Wuchapingian
Capitanian
Wordian
Roadian
Kungurian
Artinskian
Sakmarian
Asselian
Gzhelian
Kasimovian
Chang.
Wuchapingian
Capitanian
Wordian
Roadian
Kungurian
Artinskian
Sakmarian
Asselian
Gzhelian
Kasim.
La Lieude
Merifons Mbr.
Salagou
Octon Mbr.
Rabejac
Viala
Tuileres-Loiras
Usclas St. Privat
Graiss.

Figure 3

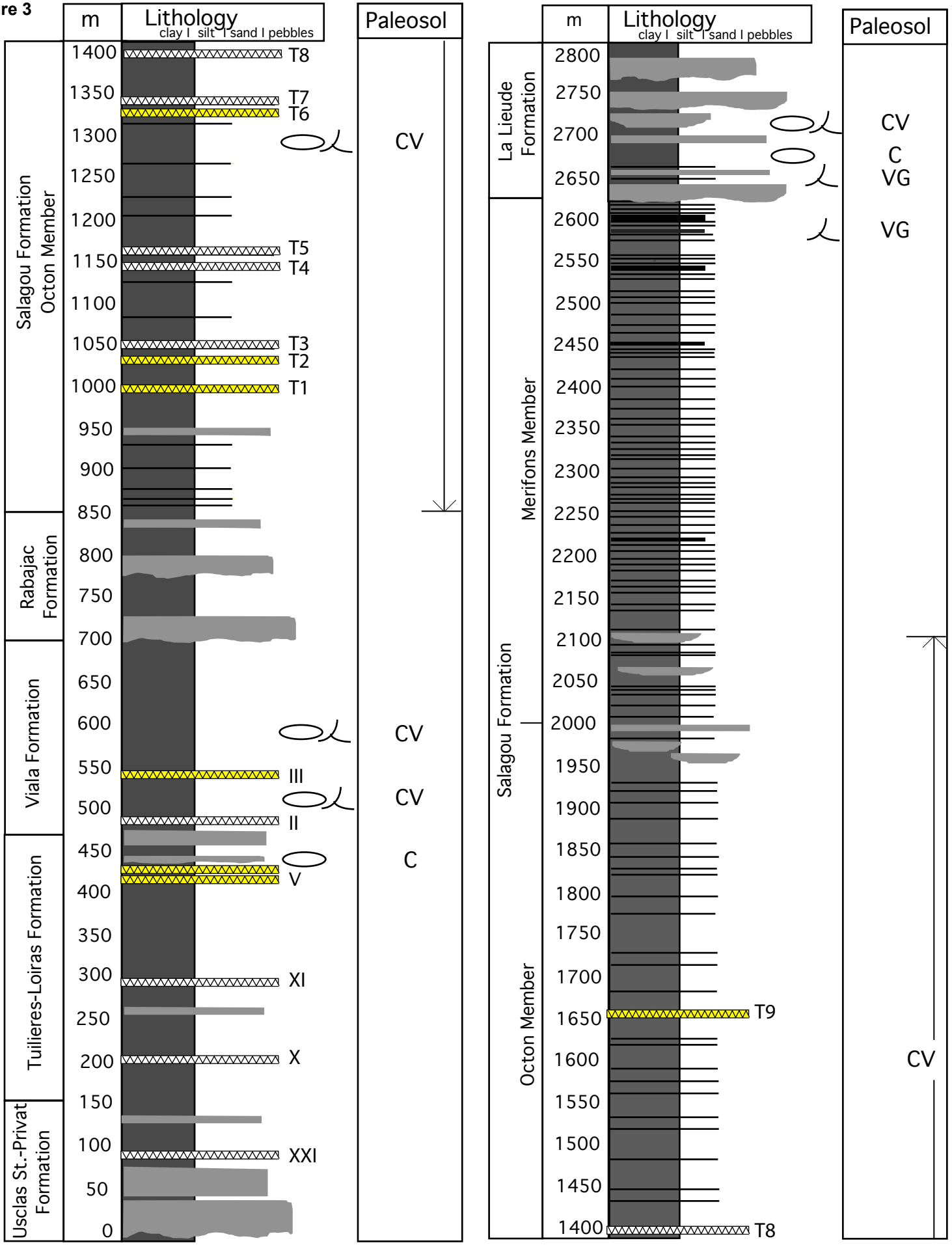

Legend

- Pedogenic Carbonate Nodules
- Slickensides
- Ash

CV Calcic Vertisol

C Calcisol

VG Vertic Gypsisol

Figure 4

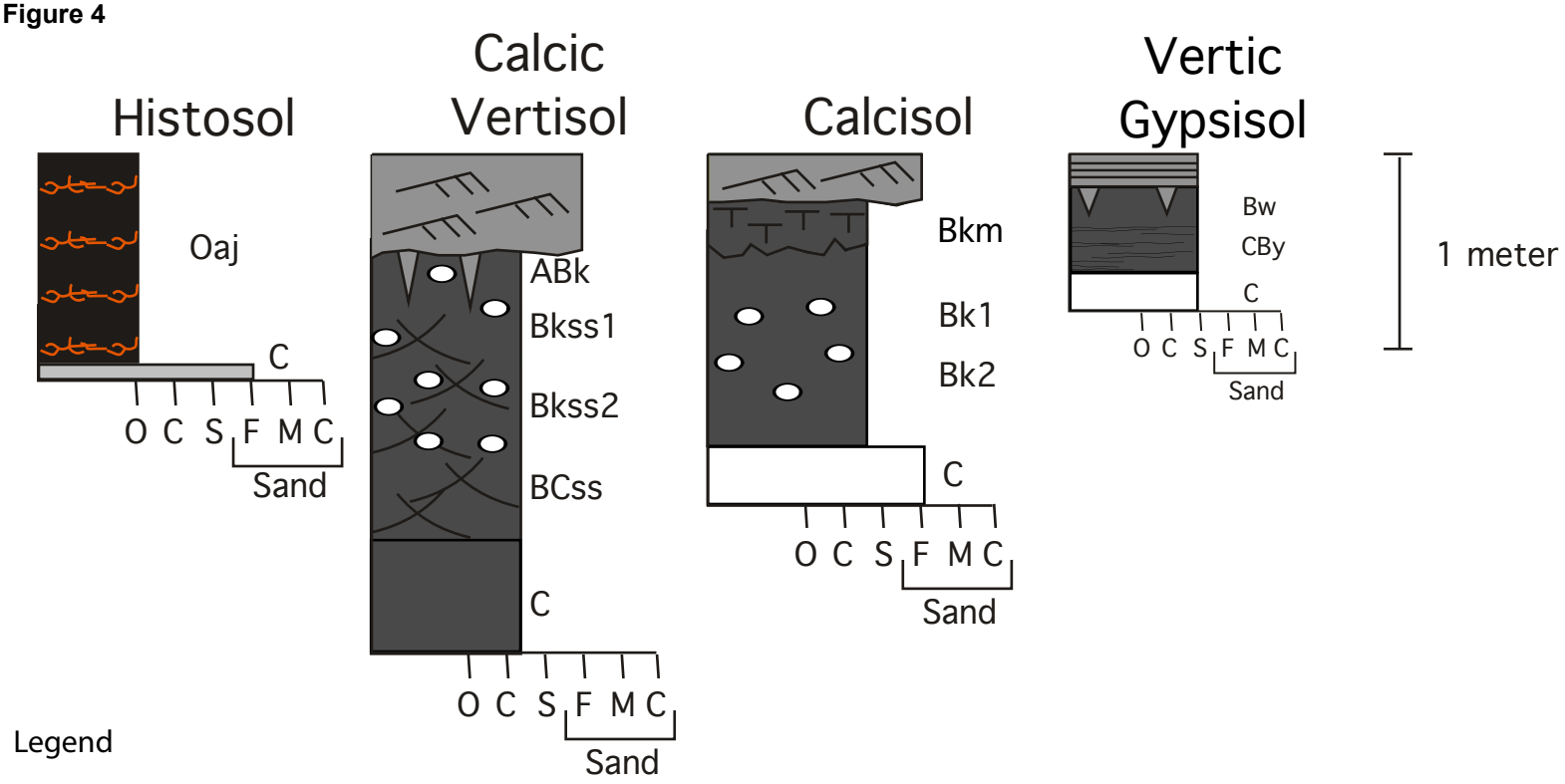

Legend

SOIL STRUCTURE

- Jarosite
- Pedogenic carbonate nodule
- Indurated Carbonate Horizon
- Slickensides
- Pedogenic Gypsum

SEDIMENTARY STRUCTURE

- Cross-bedding
- Laminations

Figure 5

Figure 6

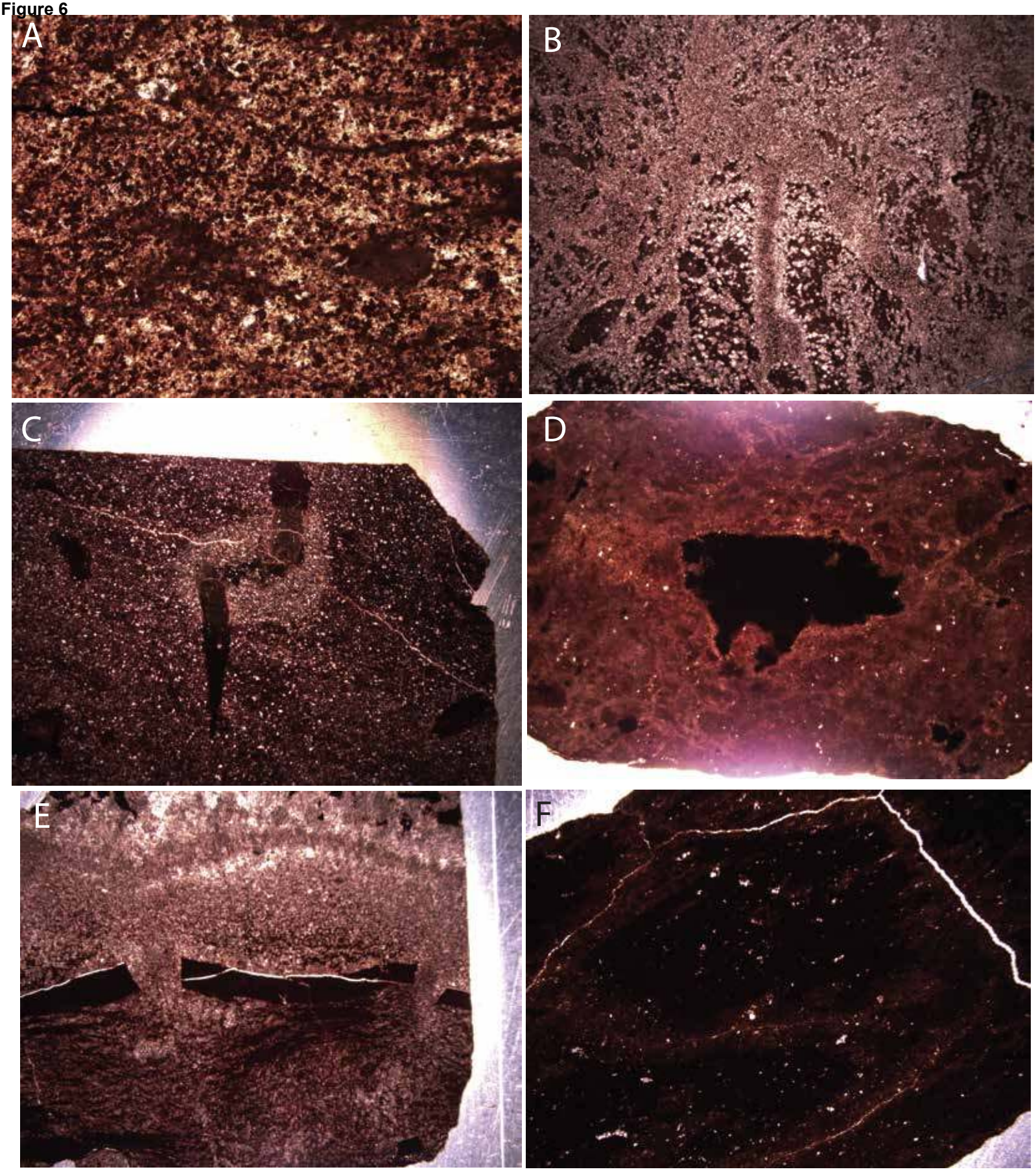

Figure 7

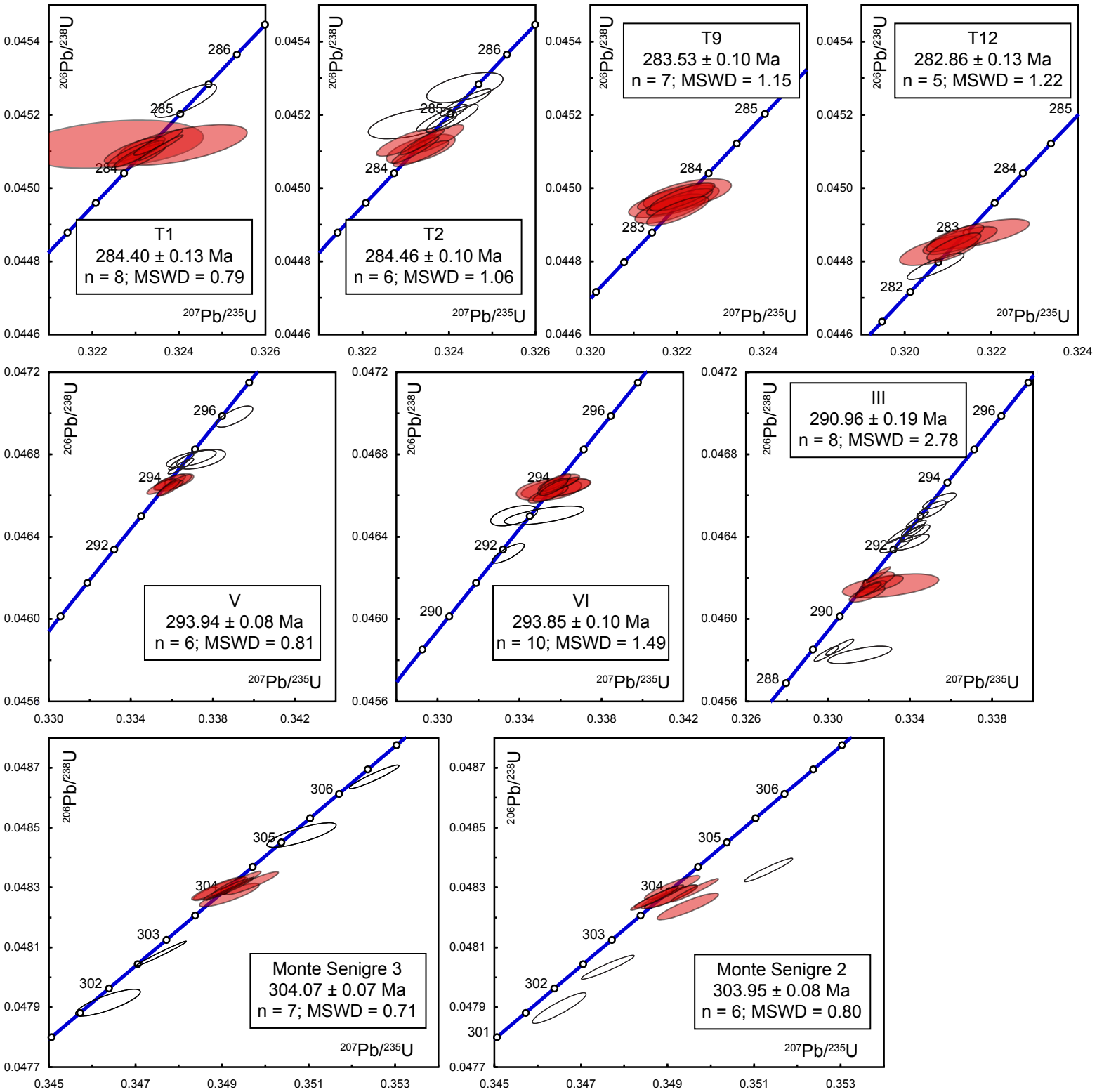
T1
284.40 ± 0.13 Ma
n = 8; MSWD = 0.79
T2
284.46 ± 0.10 Ma
n = 6; MSWD = 1.06
T9
283.53 ± 0.10 Ma
n = 7; MSWD = 1.15
T12
282.86 ± 0.13 Ma
n = 5; MSWD = 1.22
V
293.94 ± 0.08 Ma
n = 6; MSWD = 0.81
VI
293.85 ± 0.10 Ma
n = 10; MSWD = 1.49
III
290.96 ± 0.19 Ma
n = 8; MSWD = 2.78
Monte Senigre 3
304.07 ± 0.07 Ma
n = 7; MSWD = 0.71
Monte Senigre 2
303.95 ± 0.08 Ma
n = 6; MSWD = 0.80
206Pb/238U
207Pb/235U

Figure 8

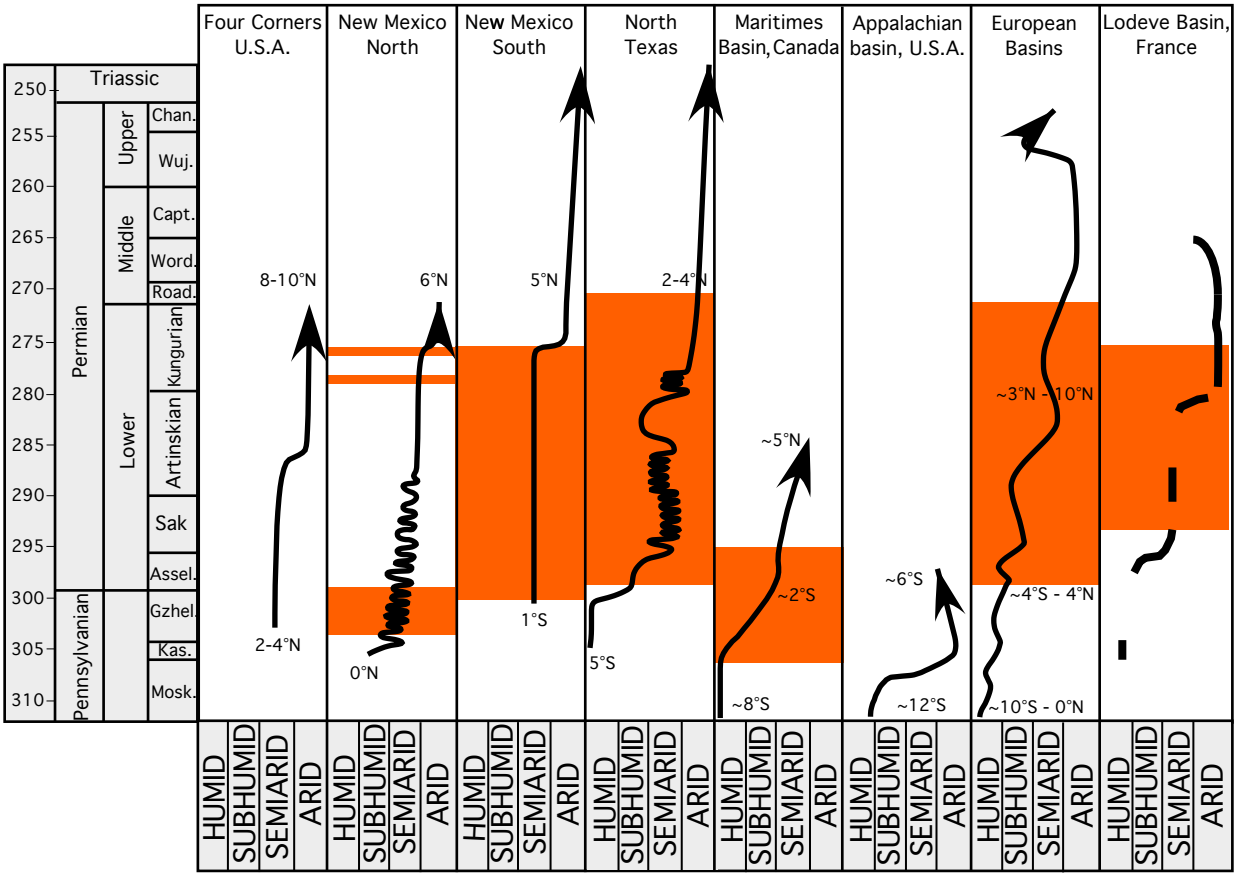

Humid = Dystric Argillisols, Histosols
Subhumid = eutric Argillisols, argillic subgroups
Semi-Arid = Calcisols, calcic subgroups
Arid = Gypsisols, gypsic subgroups, Calcisols, calcic subgroups
Extreme Seasonal Precipitation = Vertisols

Table 1. CA-TIMS U-Pb age summary

Formation Sample	Profile[1]	Latitude	Longitude	$^{206}Pb/^{238}U$ age Ma[2]	MSWD[3]	N
Salagou Formation (Octon Member)						
T12	LM 26	43.65035	3.30138	282.86 ± 0.13(0.19)[0.35]	1.22	5 of 14
T9	R VIII	43.66550	3.33481	283.53 ± 0.10(0.17)[0.34]	1.15	7 of 8
T2	R V	43.67664	3.35763	284.46 ± 0.10(0.17)[0.35]	1.06	6 of 11
T1	R V	43.67736	3.35698	284.40 ± 0.07(0.16)[0.34]	0.79	8 of 11
Viala Formation						
III	S	43.69246	3.34706	290.96 ± 0.19(0.24)[0.39]	4.28	7 of 20
Tuilières–Loiras Formation (Loiras Member)						
VI	LDCI A	43.69910	3.17872	293.85 ± 0.10(0.17)[0.36]	1.49	10 of 13
V	LDCI 25	43.69988	3.17893	293.94 ± 0.08(0.16)[0.35]	0.81	6 of 11
Graissessac Formation						
MS-2 (coal 5)	Monte Sénégra	43.68720	3.14499	303.95 ± 0.08(0.17)[0.36]	0.80	6 of 9
MS-3 (coal 4)	Monte Sénégra	43.68769	3.14536	304.07 ± 0.07(0.17)[0.36]	0.71	7 of 11

Notes: [1]Stratigraphic profiles illustrated by Schneider et al. (2006). [2]All weighted mean ages at the 95% confidence interval, as calculated from the internal 2σ errors expanded by the square root of the MSWD and the Student's T multiplier for n-1 degrees of freedom. Uncertainties are quoted as analytical (analytical+tracer) [analytical+tracer+decay constant]. [3]mean squared weighted deviations.